International Journal of Solids and Structures 46 (2009) 151–164

Contents lists available at ScienceDirect

International Journal of Solids and Structures

journal homepage: www.elsevier.com/locate/ijsolstr

Multistable composite plates with piecewise variation of lay-up in the planform

F. Mattioni *, P.M. Weaver, M.I. Friswell

Department of Aerospace Engineering, University of Bristol, Bristol BS8 1TR, UK

ARTICLE INFO

Article history:
Received 14 March 2008
Received in revised form 13 August 2008
Available online 31 August 2008

Keywords:
Bi-stable composite
Morphing structures
Non-linear analysis
Analytical methods
Thermal stress
Piecewise functions

ABSTRACT

The non-linear out-of-plane displacements of partially unsymmetric laminates are modelled using both finite element analysis and an analytical method. Attention is focused on the effects that thermal stresses have on the potential multiple shapes of a composite structure. The paper extends previous analytical models which could only take into account "free-free" boundary conditions. The shape functions that model the out-of-plane displacements are modified to include variations of the curvatures within the domain. The new analytical formulation is compared with literature and finite element analysis for a square plate and then it is tested for laminates with piecewise variation of lay-up in the planform. The results are validated against finite element analysis and experimental tests and a good correlation is obtained. Finally, a parametric study is made on the effect of changing the fibres orientation and the laminate thickness. The results confirm that it is possible to introduce bi-stable composites within structures to obtain systems that are both flexible and stiff depending on the loading environment.

1. Introduction

Composite materials made of orthotropic layers may develop residual stresses when subjected to a thermal field that varies with time (Hyer, 1982). The thermal stresses are caused by the mismatch of coefficients of thermal expansion longitudinal and transverse to the fibre direction (e.g. $o(10^{-8})$ for the longitudinal direction and $o(10^{-6})$ for the transverse direction). Furthermore, if the material is not stacked symmetrically with respect to the mid-plane, then during the cool-down from high curing temperatures, it is possible that bending and twisting moments are generated within the laminated structure, resulting in out-of-plane displacements. At room temperature, the structure has built-in residual stresses that establish equilibrium in more than one configuration. For square plates, the stable configurations are cylindrical with generators parallel to the x and y-axes and, moreover, it is possible to snap from one configuration to another by applying moments or forces to counteract the curvature. This type of behaviour presents some interesting advantages when designing structures that have the requirements of variable geometries and several studies on their applicability to morphing structures have been published (Diaconu et al., 2008; Mattioni et al., 2007; Schultz, 2008). Iqbal and Pellegrino (2000) investigated the use of bi-stable composite shells as hinges for deployable structure while Dano and Hyer (2002, 2003) and Portela et al. (2008) studied actuation systems based on piezo-electric patches. Most of the studies that can be found in the literature are focused on square or rectangular plates. Configurations different from these are usually analysed through an experimental analysis (Potter and Weaver, 2004; Gigliotti et al., 2004) or numerical simulation (Mattioni et al., 2008). Finite element analysis (FEA), in particular, is essential for preliminary studies on complex geometries and different stacking sequences but,

* Corresponding author.
E-mail addresses: filippo.mattioni@bris.ac.uk, mattioni.filippo@tiscali.it (F. Mattioni).

0020-7683/$ - see front matter © 2008 Elsevier Ltd. All rights reserved.
doi:10.1016/j.ijsolstr.2008.08.023

because of the non-linear nature of the behaviour of these plates, it is particularly time consuming and often requires continuous user input to achieve convergence. A reduced order model based on analytical techniques can be helpful to draw guidelines for the design of multi-stable structures both quickly and inexpensively. Most analytical models are based on using Rayleigh–Ritz minimisation of the total potential energy in conjunction with polynomial approximations of the displacements of the mid-plane strains (Dano and Hyer, 1998; Hufenbach and Gude, 2002; Jun and Hong, 1990). This paper extends these models to account for boundary conditions different from the free-free type so far used. Taking into account boundary conditions is essential when studying the interaction of bi-stable structures as components of larger structures and is also the first step required to be able to model different geometries with analytical techniques.

2. Analytical background

The analysis shown in this paper is based on the model by Dano and Hyer (2002) where the strain energy of an unsymmetric panel, subjected to thermal loads, is minimised by using a Rayleigh–Ritz technique to analyse the energetic content of the structure. The total potential energy (Π) of a composites structure in plane-stress and subjected to a difference in temperature, can be expressed as a function of the mid-plane strains (ε^0), of the curvatures (k^0) and of the laminate stiffness, as

$$\Pi = \int_{-\frac{l_x}{2}}^{\frac{l_x}{2}} \int_{-\frac{l_y}{2}}^{\frac{l_y}{2}} \left(\frac{1}{2} \begin{bmatrix} \underline{\varepsilon^0} \\ \underline{k^0} \end{bmatrix}^{\mathrm{T}} \begin{bmatrix} \underline{\underline{A}} & \underline{\underline{B}} \\ \underline{\underline{B}} & \underline{\underline{D}} \end{bmatrix} \begin{bmatrix} \underline{\varepsilon^0} \\ \underline{k^0} \end{bmatrix} - \begin{bmatrix} \underline{\varepsilon^0} \\ \underline{k^0} \end{bmatrix}^{\mathrm{T}} \begin{bmatrix} \underline{N^{\mathrm{th}}} \\ \underline{M^{\mathrm{th}}} \end{bmatrix} \right) \mathrm{d}x\,\mathrm{d}y, \tag{1}$$

where

$$\begin{aligned} A_{ij} &= \sum_{k=1}^{N_l} Q_{ij}^{(k)} (h_k - h_{k-1}), \\ B_{ij} &= \frac{1}{2} \sum_{k=1}^{N_l} Q_{ij}^{(k)} (h_k^2 - h_{k-1}^2), \\ D_{ij} &= \frac{1}{3} \sum_{k=1}^{N_l} Q_{ij}^{(k)} (h_k^3 - h_{k-1}^3) \end{aligned} \tag{2}$$

are the laminate stiffness matrices, $Q_{ij}^{(k)}$ is the reduced stiffness matrix of the kth layer according to Jones (1999) and

$$\begin{aligned} N_i^{\mathrm{th}} &= \sum_{k=1}^{N_l} \sum_{j=1}^{N} Q_{ij}^{(k)} \alpha_j^{(k)} (h_k - h_{k-1}) \Delta T, \\ M_i^{\mathrm{th}} &= \tfrac{1}{2} \sum_{k=1}^{N_l} \sum_{j=1}^{N} Q_{ij}^{(k)} \alpha_j^{(k)} (h_k^2 - h_{k-1}^2) \Delta T \end{aligned} \tag{3}$$

are the thermal forces and moments per unit length. In order to be able to predict the stable configurations after cool-down, the mid-plane strain components ε^0 and κ^0 are expressed as polynomial functions with unknown coefficients that have to be determined by minimising the total potential energy. It is noteworthy that the function chosen for the approximation must satisfy at least the essential boundary conditions. The approximation function chosen by Hyer to model the out-of-plane displacement is

$$w(x,y) = -\frac{1}{2}(w_{20}x^2 + w_{02}y^2 + w_{11}xy), \tag{4}$$

where w_{20}, w_{02}, w_{11} are unknown coefficients which represent, respectively, the negative of the curvatures in the x and y directions and the negative of the twist curvature, as

$$k_x^0 = -\frac{\partial^2 w^0}{\partial x^2} = w_{20}, \quad k_y^0 = -\frac{\partial^2 w^0}{\partial y^2} = w_{02}, \quad k_{xy}^0 = -2\frac{\partial^2 w^0}{\partial x \partial y} = w_{11}. \tag{5}$$

This choice of displacement function assumes the curvature to be constant throughout the domain. To obtain the shear deformation γ_{xy}^0, compatibility relations are applied. The total strain vector $\varepsilon = \varepsilon^0 + z\kappa^0$ includes von Kàrman non-linear terms for the mid-plane strains. This requirement is a mandatory feature as Hyer and Bhavani (1984) showed that the classical lamination theory fails to capture the room-temperature shape of cross-ply laminates. The mid-plane strain vector formulation then becomes

$$\underline{\varepsilon}^0 = \begin{Bmatrix} \varepsilon_x^0 \\ \varepsilon_y^0 \\ \gamma_{xy}^0 \end{Bmatrix} = \begin{Bmatrix} \dfrac{\partial u^0}{\partial x} + \dfrac{1}{2}\left(\dfrac{\partial w^0}{\partial x}\right)^2 \\ \dfrac{\partial v^0}{\partial y} + \dfrac{1}{2}\left(\dfrac{\partial w^0}{\partial y}\right)^2 \\ \dfrac{\partial u^0}{\partial y} + \dfrac{\partial v^0}{\partial x} + \dfrac{\partial w^0}{\partial x}\dfrac{\partial w^0}{\partial y} \end{Bmatrix}, \tag{6}$$

while the curvature vector is

$$\underline{k}^0 = -\begin{Bmatrix} w_{20} \\ w_{02} \\ w_{11} \end{Bmatrix}. \tag{7}$$

Dano and Hyer (2002) assumed that the strain is given by

$$\begin{aligned} \varepsilon_x^0 &= \varepsilon_{x00} + \varepsilon_{x20}x^2 + \varepsilon_{x11}xy + \varepsilon_{x02}y^2, \\ \varepsilon_y^0 &= \varepsilon_{y00} + \varepsilon_{y20}x^2 + \varepsilon_{y11}xy + \varepsilon_{y02}y^2. \end{aligned} \tag{8}$$

The in-plane displacement function is then

$$\begin{aligned} u^0(x,y) &= \int \left[\varepsilon_x^0 - \frac{1}{2}\left(\frac{\partial w^0}{\partial x}\right)^2 \right] \mathrm{d}x + u_{01}y + u_{03}y^3, \\ v^0(x,y) &= \int \left[\varepsilon_y^0 - \frac{1}{2}\left(\frac{\partial w^0}{\partial y}\right)^2 \right] \mathrm{d}y + v_{10}x + v_{30}x^3. \end{aligned} \tag{9}$$

The unknown functions $h(y) = u_{01}y + u_{03}y^3$ and $h(y) = v_{10}x + v_{30}x^3$ are chosen to obtain the required degrees of freedom for the displacements. Rigid body rotations are eliminated by equating the coefficients of the first order terms of the variables x and y. The shear strain deformation is simply

$$\gamma_{xy}^0 = \frac{\partial u^0}{\partial y} + \frac{\partial v^0}{\partial x} + \frac{\partial w^0}{\partial x}\frac{\partial w^0}{\partial y}. \tag{10}$$

3. Extension of the existing models

As shown in Section 2, the procedure to express the total potential energy Π as a function of the displacement coefficients, material properties and temperature change, is well-established and so far it has been successfully applied to panels with uniform stacking sequence. The study presented herein modifies the existing models to consider piecewise variation of the lay-up in the planform, thus accounting for boundary conditions embedded into the structure. The purpose is to provide an engineering tool that can help at the preliminary design stage of unsymmetrical laminated structures. With such a model it is possible to analyse the equilibrium configurations of structures for more practical applications, such as those described by Diaconu et al. (2008).

It has been observed that, to model boundary conditions that are not simply free edges, the hypothesis of constant curvatures has to be removed since it is too restrictive. This is clearly understood by examining the bending behaviour of a plate in the region close to the edge where a constraining moment is applied. From the kinematics it is known that the bending moment in a plate is proportional to the curvature and therefore whenever a moment is applied to an edge, a variation in the local curvature is expected. For this reason the curvature must be allowed to vary across the domain and therefore a fourth order displacement function is chosen as a basis to extend the model. The out-of-plane displacement function can be regarded as the result of the product of two parabolas along the principal directions (i.e. parabolic variation of the curvatures)

$$w(x,y) = P(x) \cdot G(y), \tag{11}$$

where

$$\begin{aligned} P(x) &= p_0 + p_1x + p_2x^2, \\ G(y) &= g_0 + g_1y + g_2y^2. \end{aligned} \tag{12}$$

To simplify the computation of derivatives and integrals, the previous expression is re-arranged as

$$w(x,y) = w_{00} + w_{10}x + w_{01}y + w_{20}x^2 + w_{02}y^2 + w_{11}xy + w_{12}xy^2 + w_{21}x^2y + w_{22}x^2y^2. \tag{13}$$

Within this notation, the first subscript refers to the order of the x-variable while the second one refers to the order of the y-variable. The polynomial functions chosen by Hyer to model the strain displacements provide an adequate number of degrees of freedom and therefore their expression is unchanged. For completeness they are presented, with the different notation adopted here, as

$$\begin{aligned} \varepsilon_x^0 &= \varepsilon_{x00} + \varepsilon_{x20}x^2 + \varepsilon_{x11}xy + \varepsilon_{x02}y^2, \\ \varepsilon_y^0 &= \varepsilon_{y00} + \varepsilon_{y20}x^2 + \varepsilon_{y11}xy + \varepsilon_{y02}y^2. \end{aligned} \tag{14}$$

The shear deformation is determined using the procedure outlined in Eqs. (9) and (10). The drilling degree of freedom is eliminated by imposing $u_{01} = v_{10}$. This model has 20 unknown coefficients.

4. Application to a square plate

To validate the effectiveness of the modified model and before applying it to more complex types of structures, it is applied to a square plate with all edges free. The results obtained are then compared with Hyer's model and FEA. The total potential energy is assembled and minimised with the help of the symbolic manipulation software *Maple 9.5*. The equilibrium configurations are obtained by using a non-linear optimisation subroutine "`NLPSolve`" that finds the local minima of a non-linear function. This greatly simplifies the solution of the system of non-linear equations that are obtained when minimising the total energy. Furthermore, the boundary conditions and the other constraints imposed on the model can be directly implemented as constraints for the optimisation process. In this way, it is easier to automate the process for parametric studies and it is possible to avoid the difficulties encountered when finding the solution through a Newton–Räphson scheme (typically the sensitivity with respect to the initial guess). The comparison is carried out for a square plate with side length L of 180 mm and stacking sequence $[0_4/90_4]_T$. Table 1 shows the values of the total potential energy and of the principal curvatures (k_x and k_y) for the two equilibrium configurations. Fig. 1 shows a superposition of the three equilibrium shapes obtained respectively with Hyer's model, the extended model and FEA. Fig. 2 shows three sections of the plate obtained at the centre and at 80% of the semi-span of the panel, respectively. To highlight the differences between the three models the vertical displacement has been amplified by a factor of 5. As can be seen, the differences between the three models are very small all over the panel and the greater difference is found within the regions close to the edges. Here, the configuration computed with the higher order model has a slight parabolic variation of the edge shape, whereas the panel obtained with Hyer's model shows an almost perfectly straight edge. The FEA predicts an edge that is almost flat in the

Table 1
Curvature comparison for the square plate

		Hyer's model (m^{-1})	Extended model (m^{-1})
Configuration 1	Π	−0.874	−0.878
	k_x	−3.52	$-28.02y^2 + 3.58$
	k_y	0.04	$-28.02x^2 + 0.0089$
Configuration 2	Π	−0.874	−0.878
	k_x	0.04	$-28.02x^2 + 0.0089$
	k_y	−3.52	$-28.02y^2 + 3.58$

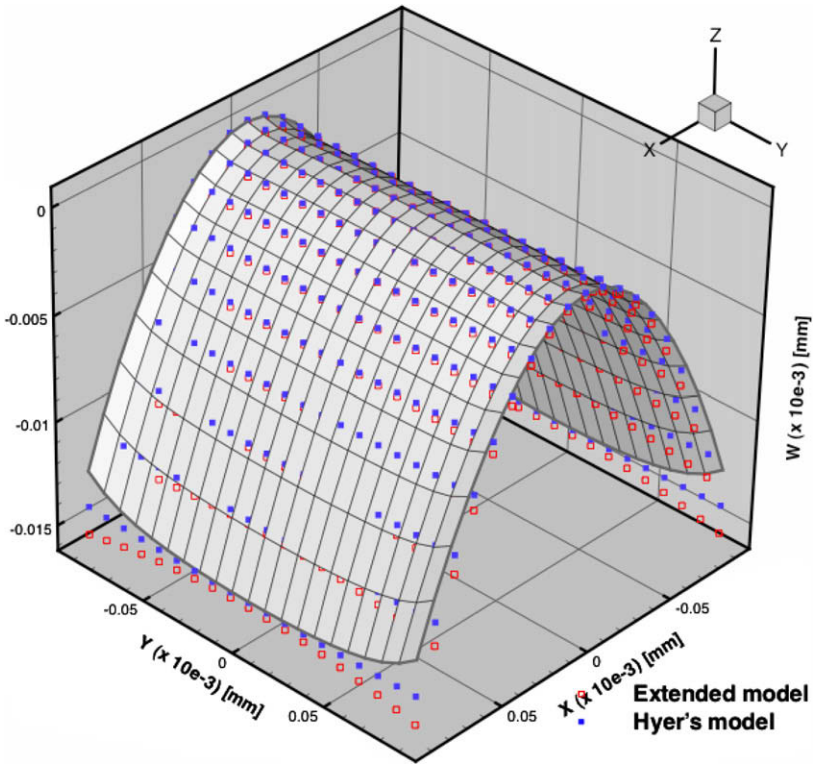

Fig. 1. Hyer's model and extended model overlaid onto the FE model.

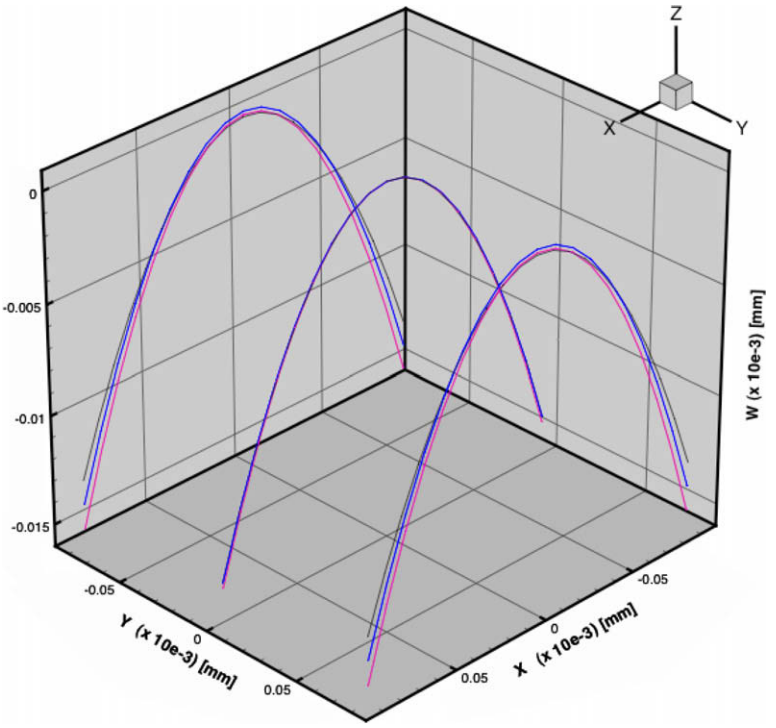

Fig. 2. Cross-section comparison at different stations.

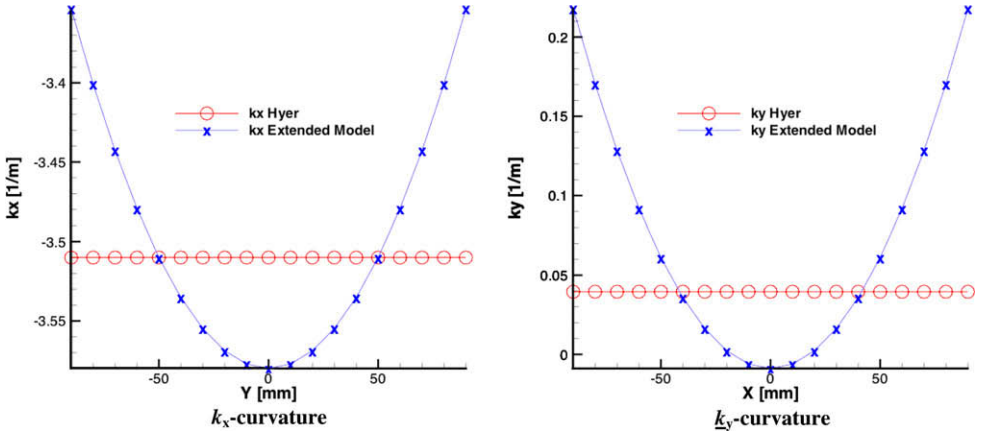

Fig. 3. Principal curvatures comparison.

central part and slightly curved towards the corners. In this area, the displacements are particularly difficult to match with those obtained with the FEA because of the steep variation of the curvatures. Both the model developed by Hyer and its extension are not able to describe accurately the local displacement in this region since they have been developed to obtain a good approximation of the overall deformation and not of the local effects close to the boundary. A detailed analysis of the boundary layer area requires a different type of approximation functions and it is beyond the scope of this study. Fig. 3 shows a comparison of the values of the curvatures for the two analytical models at a section taken at the centre of the plate. It is clear that the higher order model predicts quadratic curvature while the previous model has a constant value throughout the domain.

5. Application to a compound plate

The results obtained for the square plate show a satisfactory agreement between the two analytical models and therefore the higher order model is applied to the analysis of panels with piecewise variation of the laminate in the planform. A test structure for this purpose is obtained by joining together two square plates with different stacking sequences. The panel is

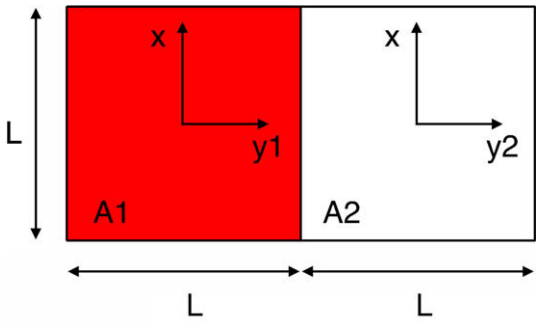

Fig. 4. Test model geometry and coordinate system.

180 mm × 360 mm and the coordinate systems used throughout this section are shown in Fig. 4. The material properties are those of typical pre-preg carbon–epoxy laminates and are listed in Table 2. The left-hand side of the plate has a symmetric stacking sequence $(0_2/90_2]_{SYM})$ while the right-hand side has an unsymmetric lay-up $(0_4/90_4]_T)$. This is equivalent to imposing an elastic boundary condition at the edge where the two plates are joined together. An experimental demonstrator of the aforementioned structure has been built and its equilibrium configurations are shown in Fig. 5.

Let A be the domain representing the whole structure so that $A = A_1 \cup A_2$, where A_1 represents the symmetric plate and A_2 the unsymmetric plate. Using a domain decomposition, if the functions that describe the displacements are piecewise smooth over the domain A, it is possible to take into account the interaction between the symmetric and unsymmetric portions of plate. The displacement field of each part of the panel is modeled according to Eqs. (9) and (14). For clarity, the function for the assumed out-of-plane displacement for each plate is presented

$$w(x,y_i)^{(i)} = w_{00}^{(i)} + w_{10}^{(i)}x + w_{01}^{(i)}y_i + w_{20}^{(i)}x^2 + w_{02}^{(i)}y_i^2 + w_{11}^{(i)}xy_i + + w_{12}^{(i)}xy_i^2 + w_{21}^{(i)}x^2y_i + w_{22}^{(i)}x^2y_i^2, \tag{15}$$

whilst the strain functions are

$$\begin{aligned} \varepsilon_x^{0(i)} &= \varepsilon_{x00}^{(i)} + \varepsilon_{x20}^{(i)}x^2 + \varepsilon_{x11}^{(i)}xy_i + \varepsilon_{x02}^{(i)}y_i^2, \\ \varepsilon_y^{0(i)} &= \varepsilon_{y00}^{(i)} + \varepsilon_{y20}^{(i)}x^2 + \varepsilon_{y11}^{(i)}xy_i + \varepsilon_{y02}^{(i)}y_i^2, \end{aligned} \tag{16}$$

where the superscript i refers to the symmetric ($i = 1$) or unsymmetric ($i = 2$) part. The strain energy is formulated for each substructure separately, thus accounting for the different stacking sequences, and then the two contributions are summed to obtain the energy for the complete structure, $\Pi = \Pi_1 + \Pi_2$.

$$\Pi = \int\int_{A_1} \left(\frac{1}{2} \begin{bmatrix} \underline{\varepsilon}^{(1)} \\ \underline{k}^{(1)} \end{bmatrix}^{\mathrm{T}} \begin{bmatrix} \underline{\underline{A}} & \underline{\underline{B}} \\ \underline{\underline{B}} & \underline{\underline{D}} \end{bmatrix}^{(1)} \begin{bmatrix} \underline{\varepsilon}^{(1)} \\ \underline{k}^{(1)} \end{bmatrix} - \begin{bmatrix} \underline{\varepsilon}^{(1)} \\ \underline{k}^{(1)} \end{bmatrix}^{\mathrm{T}} \begin{bmatrix} \underline{N}^{\mathrm{th}} \\ \underline{M}^{\mathrm{th}} \end{bmatrix}^{(1)} \right) \mathrm{d}x\mathrm{d}y + \int\int_{A_2} \left(\frac{1}{2} \begin{bmatrix} \underline{\varepsilon}^{(2)} \\ \underline{k}^{(2)} \end{bmatrix}^{\mathrm{T}} \begin{bmatrix} \underline{\underline{A}} & \underline{\underline{B}} \\ \underline{\underline{B}} & \underline{\underline{D}} \end{bmatrix}^{(2)} \begin{bmatrix} \underline{\varepsilon}^{(2)} \\ \underline{k}^{(2)} \end{bmatrix} - \begin{bmatrix} \underline{\varepsilon}^{(2)} \\ \underline{k}^{(2)} \end{bmatrix}^{\mathrm{T}} \begin{bmatrix} \underline{N}^{\mathrm{th}} \\ \underline{M}^{\mathrm{th}} \end{bmatrix}^{(2)} \right) \mathrm{d}x\mathrm{d}y. \tag{17}$$

Table 2
Typical values for the material properties used throughout the paper

Material	E_{11} (GPa)	E_{22} (GPa)	G_{12} (GPa)	ν_{12}	α_1 (°C^{-1})	α_2 (°C^{-1})	t (mm)
T300/914	130	10	4.4	0.33	−0.18e − 6	30e − 6	0.125

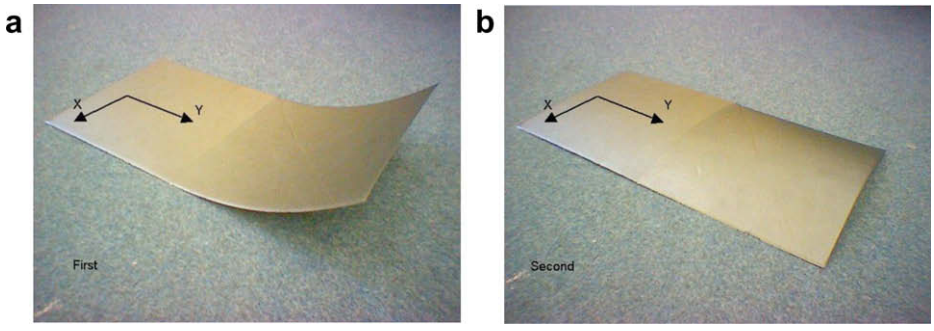

Fig. 5. Experimental model. (a) First equilibrium shape. (b) Second equilibrium shape.

The strain energy Π is now a function of 42 unknown coefficients and its local minima correspond to the equilibrium configurations of the plate. To simplify the minimisation process, the following assumptions are made

- The geometric centre of the symmetric part is clamped to eliminate rigid body translation (i.e. $w_{00}^{(1)} = 0$).
- From the experimental observation, it has been noticed that the equilibrium configurations are symmetric with respect to the y-axis (i.e. $w_{10}^{(i)} = w_{11}^{(i)} = w_{12}^{(i)} = 0$ for $i = 1,2$).
- The drilling degree of freedom is eliminated in both parts (i.e. $u_{01}^{(i)} = v_{10}^{(i)}$ for $i = 1,2$).

With this approach, the number of unknown coefficients is reduced to 33. To account for the interaction between the symmetric part and the unsymmetric part of the panel, it is necessary to impose the continuity of the displacement across the whole domain A, and therefore the following conditions must hold:

$$\begin{aligned} u^{(1)}\left(x,\frac{L}{2}\right) &= u^{(2)}\left(x,-\frac{L}{2}\right),\\ v^{(1)}\left(x,\frac{L}{2}\right) &= v^{(2)}\left(x,-\frac{L}{2}\right),\\ w^{(1)}\left(x,\frac{L}{2}\right) &= w^{(2)}\left(x,-\frac{L}{2}\right),\\ \frac{\partial w^{(1)}}{\partial x}\left(x,\frac{L}{2}\right) &= \frac{\partial w^{(2)}}{\partial x}\left(x,-\frac{L}{2}\right). \end{aligned} \tag{18}$$

The continuity on $\partial w/\partial y$ is not imposed since this is implicitly satisfied from within the continuity of the out-of-plane displacement. The solutions have been found with the same technique as for the square plate. The analytical model successfully captures the behaviour of the multi-stable structure as shown in Fig. 6.

It must be pointed out that Eq. (18) are assumed to be valid on a macroscopic basis (i.e. at laminate level). The understanding of what happens at ply level requires a different approach. Because of the particular stacking sequence, fibres and matrix continuity at ply level can only be obtained for those layers with fibres at 0^0 (i.e. parallel to the y-axis), which are continuous through the symmetric and the unsymmetric laminates. For the layers at 90°, such continuity relies entirely on the matrix since the fibres are parallel to the boundary. This creates resin-rich zones that also induce stress-concentrations that might cause cracks to develop when the load axis is along the 0° direction. To reduce this, it is possible to modify the interface between the two parts by offsetting the position of the ply drop for the layers at 90°. This would create a transition zone rather that an abrupt change as it is now, but could also modify the stiffness of the constraint introducing further difficulties for the analytical model. For these reasons, for engineering modelling purposes, the assumption of structural continuity at laminate level is considered acceptable.

A detailed comparison with the numerical and experimental configurations is presented in the following section.

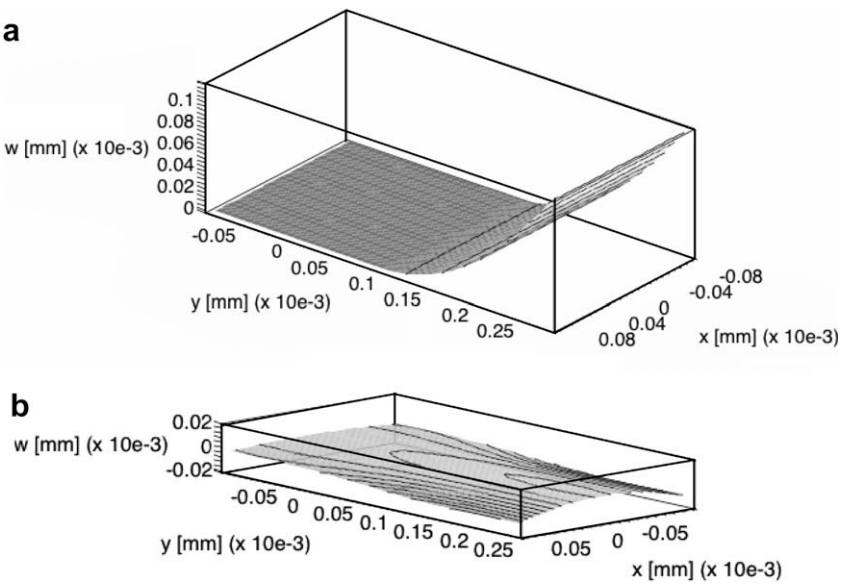

Fig. 6. Equilibrium shapes obtained with the analytical model. (a) First equilibrium shape. (b) Second equilibrium shape.

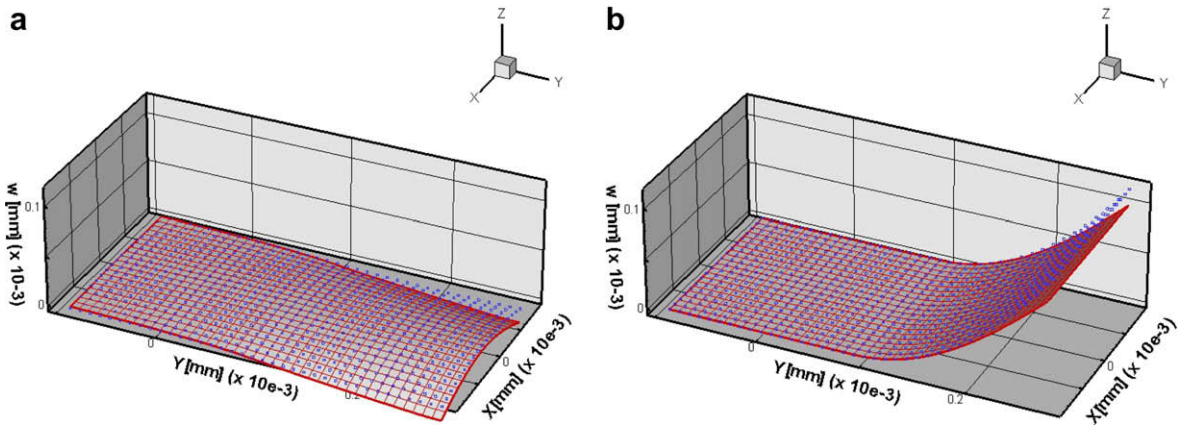

Fig. 7. Analytical vs FE shape for the 4-layered plate. (a) Flat configuration. (b) Curled configuration.

6. Finite element analysis and experimental results

In this section, the results obtained with the analytical model and their comparison with numerical and experimental data is presented. Residual stresses are generated by the temperature difference and no external force is applied to the specimen. Since there is more than one equilibrium configuration, the main difficulty is presented by the existence of a bifurcation point, a value for the temperature beyond which two solutions are possible. The general approach is to impose a geometric imperfection to the structure, to coax it to converge to one configuration rather than the other. This approach generally works well for square plates where removing the double symmetry coaxes the algorithm to converge to one solution. However, for the chosen configuration there is no such symmetry, the sensitivity with respect to imperfections is less evident and therefore a different method was required. It has been observed that the static algorithm converges to one equilibrium shape whereas the dynamic algorithm always converges to the other shape. This difference is due to the inertia contribution, which the dynamic analysis accounts for (Mattioni et al., 2007). This evidence suggested that using a pseudo-dynamic solution scheme it could be possible to converge to either of the equilibrium states by modifying the amount of artificial damping used. FEA has been performed with the commercial software ABAQUS where the pseudo dynamic analysis is performed by using the "`*Static, stabilize`" option which makes use of an automatic stabilisation based on the addition of viscous forces to the global equilibrium equation. The viscous forces are introduced into the numerical scheme as soon as instabilities are detected in the stiffness matrix of the system and have the form of $F_v = cM^*v$, where M^* is the artificial mass matrix calculated with unit density, c is the damping factor chosen as a fraction of the dissipated energy and v is the vector of nodal velocities. This stabilisation technique is, in fact, equivalent to adding the inertia contribution only for those numerical steps that would otherwise present singularities. A more detailed description of the numerical analysis procedure is given in Mattioni et al. (2007). The panel is modelled using 800 four-node-square shell elements (S4R) with a total of 861 nodes and 5166 degrees of freedom. The cool-down is simulated by applying an initial temperature of 140 °C and a final temperature of 0 °C to all the nodes of the model. If no stabilisation is used, the solution analysis always converges to one of the equilibrium shapes and "negative eigenvalue warnings" are issued by the solver. This confirms the presence of a singular point and that the algorithm followed one branch of the solution until convergence is achieved. To capture the second equilibrium shape, a separate analysis makes use of the "stabilize" option. The stabilisation technique adds viscous forces to damp local instabilities when convergence is difficult to achieve and allows the system to jump to the other branch of the solution and to converge to the other equilibrium shape.

Figs. 7 and 8 show an overall comparison between the FEA and the analytical data for the 4- and the 8-layered panels. The comparison is carried out according to the system of reference shown in Fig. 9. The markers represent the analytical data, whereas the mesh represents the FEA results. As can be seen, the two models have a satisfactory overall agreement, the greatest difference being towards the unsymmetric edge. The 8-layered panel shows a better agreement compared to the 4-layered one. The analytical model, because of its reduced number of degrees of freedom, is in a sense stiffer and therefore it better captures the reduced displacements of the 8-layered panel. Figs. 10 and 11 show a similar comparison but the results are also compared against experimental data. This latter comparison highlights the effect that the FEA is also stiffer with respect to experimental data, presumably due to the mesh density chosen as a compromise between accuracy and computational efficiency.

7. Parametric studies: effects of boundary conditions

In this section, the analytical model is used to investigate the effects of different lay-ups and thicknesses of the symmetric part of panel. The scope of this section is to highlight the effect of the boundary conditions on the bi-stable

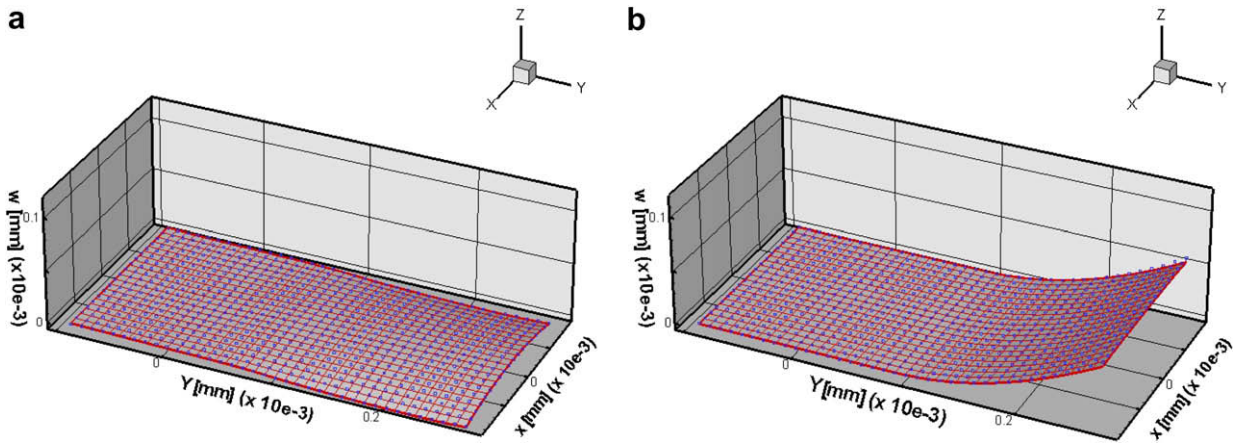

Fig. 8. Analytical vs FE shape for the 8-layered plate. (a) Flat configuration. (b) Curled configuration.

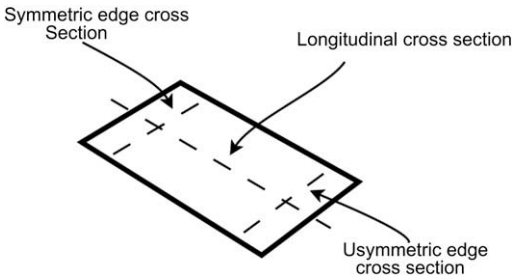

Fig. 9. Test model geometry and coordinate system.

properties of the unsymmetric part of the panel. The base state is represented by the 8-layered unsymmetric panel without any constraint. As observed in the previous sections, the two cylindrical configurations that are obtained with a square unsymmetric panel are identical in terms of curvature values. By constraining one of the edges of the panel, the curvature along the constrained edge is considerably reduced, as expected. At the boundary between the two 8-layered plates, the transverse curvature is 37% of the unrestrained panel curvature. Moving away from the restrained edge, the effect of the constraint diminishes and the curvature is gradually recovered. At the maximum distance from the constraint (i.e. the "unsymmetric-edge"), the curvature reaches approximately 60% of the unrestrained plate curvature. By examining the longitudinal curvature (i.e. perpendicular to the constrained edge), the curvature is 99% of the value achieved by the free panel (i.e. it is almost unaffected by the presence of the symmetric panel). This effect is explained by the fact that the constraint increases the stiffness in the transverse direction and therefore the associated curvature changes. Along the longitudinal direction, the shape is almost perfectly cylindrical, there is little transverse curvature and therefore a very small effect is observed. In fact, the shape is never exactly cylindrical but has a small anticlastic component that is highly dependent on the thickness/side-length ratio. For plates with geometry similar to those analysed here, it is expected that this response does not affect the global behaviour of the panel and therefore as a first approximation, the effects of the anticlastic curvature are neglected.

The parametric study was done using seven different panels with different lay-ups for the symmetric part:

- 8 layers: $[0°_2, 90°_2]_{SYM}$
- 16 layers: $[0°_4, 90°_4]_{SYM}$
- 24 layers: $[0°_6, 90°_6]_{SYM}$
- Ninety dominant laminate: $[90°_3, 0°]_{SYM}$
- Zero dominant laminate: $[0°_3, 90°]_{SYM}$
- Quasi-isotropic laminate: $[45°, -45°, 90°, 0°]_{SYM}$
- Antisymmetric angle ply: $[45°, -45°_2, 45°]_{ANTISYM}$

The principal difference between the laminates tested is the transverse stiffness. For the first three stacking sequences, the driving factor is the thickness, while for the last four it is the fibre orientation. Throughout the analysis the unsymmetric part

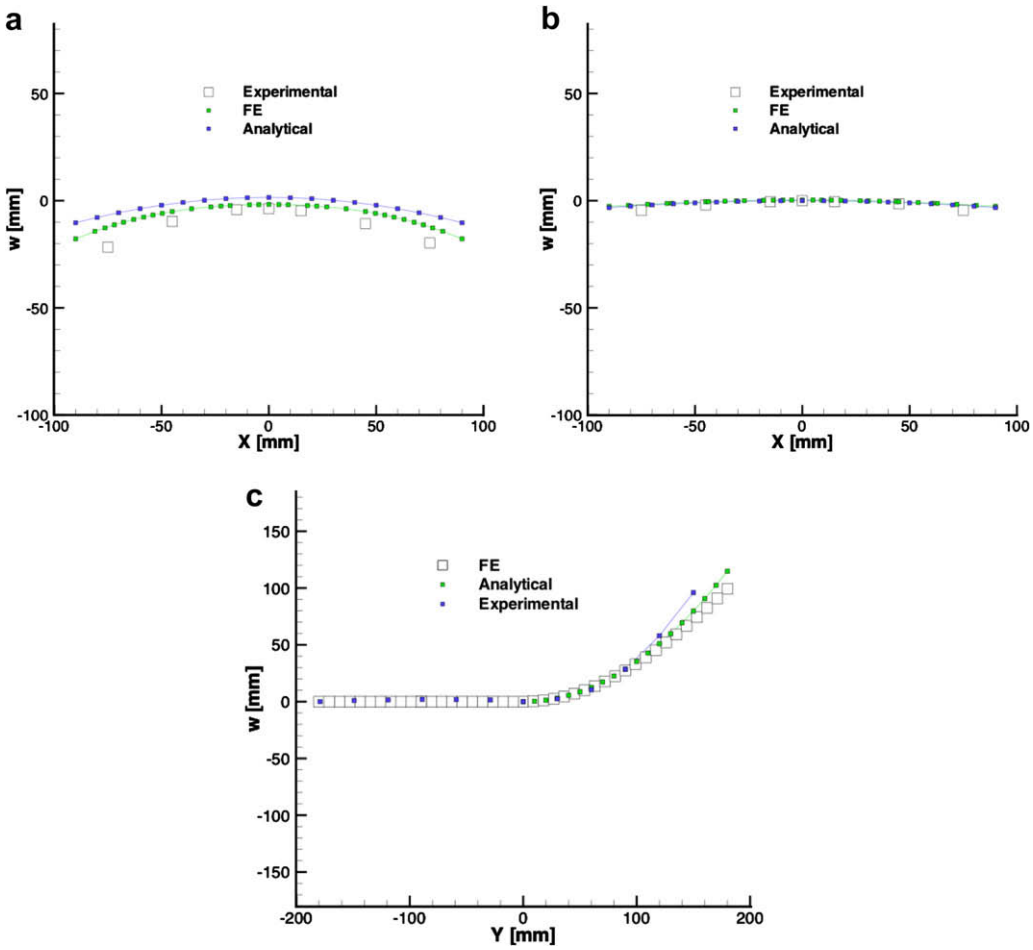

Fig. 10. Analytical vs. FEA section for the 4-layered plate. (a) Unsymmetric edge cross-section. (b) Symmetric edge cross-section. (c) Longitudinal cross-section for the curled configuration.

remains unchanged, with stacking sequence $[90°_4, 0°_4]_T$, as this maximises the bi-stable behaviour. The values of the transverse curvature k_x and the difference with respect to the free-free square plate are shown in Tables 3 and 4. From a physical point of view it is easier to understand the differences by examining Figs. 13 and 14 where the different cross-sections (see Fig. 12) of the plate are shown.

Fig. 13 presents the results obtained by varying the number of layers. As expected, an increase in thickness results in a reduction of the transverse curvature of the flat configuration as shown by Fig. 13(a) and (b). Fig. 13(c) shows almost identical values for all configurations and this result confirms the reduced sensitivity of the longitudinal curvature with respect to a variation of the constraint characteristics.

The effects of using different stacking sequences with the symmetric panel are summarised in Fig. 14. Fig. 14(a) and (b) shows the same result as above but with a much smaller range of variation since the thickness of the two plates is the same. Fig. 14(c) shows (Fig. 13(c) likewise) that the longitudinal curvature is not affected by the constraint. In both cases, the curvature at the unsymmetric edge is very similar and reaches approximately 60% of the unrestrained panel. These results highlight the robustness of the bi-stable behaviour of unsymmetric laminates. Even if one of the edges is constrained, almost 60% of their bi-stable behaviour is retained and moreover it is possible to tailor the final geometry with reasonable accuracy.

8. Concluding remarks

A non-linear analytical model to predict the equilibrium configurations of multistable composite with piecewise variation of the laminate in the planform has been presented.

The model is aimed at helping the preliminary design phases of unsymmetric laminates and is based on an empirical approach that relies on experimental tests to validate the results. The goal was to extend previous analytical techniques

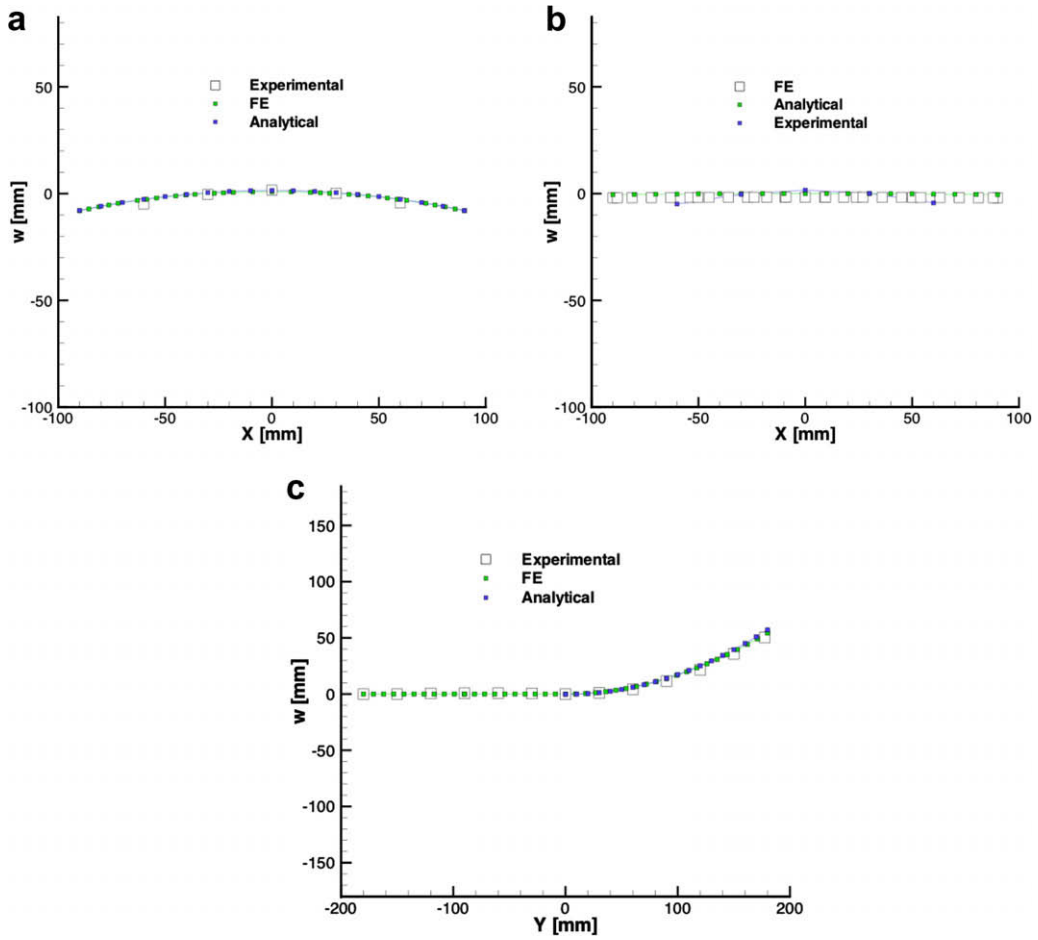

Fig. 11. Analytical vs. FE section for the 8-layered plate. (a) Unsymmetric edge cross-section. (b) Symmetric edge cross-section. (c) Longitudinal cross-section for the curled configuration.

Table 3
Transverse curvatures k_x for different thicknesses

	Constrained cross-section (m^{-1})	Δ%	Unsymmetric cross-section (m^{-1})	Δ%
8 layers	−1.25	37.2	−2.03	60.5
16 layers	−0.67	20.0	−2.04	60.9
24 layers	−0.33	9.8	−2.03	60.5
Reference	Square plate k_x	−3.351		

Table 4
Transverse curvatures k_x for different laminates

	Constrained cross-section (m^{-1})	Δ%	Unsymmetric cross-section (m^{-1})	Δ%
$[0_2°, 90_2°]_{SYM}$	−1.25	37.2	−2.03	60.5
$[0°_3, 90°]_{SYM}$	−2.25	67.0	−2.76	82.2
$[90°_3, 90°]_{SYM}$	−1.21	36.1	−2.01	60.1
$[45°, -45°_2, 45°]_{ANTISYM}$	−1.56	46.6	−2.32	69.2
$[45°, -45°, 90, 0°]_{SYM}$	−1.56	46.6	−2.32	69.2
Reference	Square plate k_x	−3.351		

by adding the capability to map curvatures that are non-constant within the domain. A new formulation for the displacement field is undertaken and used to predict the deformation of a bi-stable square plate. The results have been validated against previous models and FEA. The extended model is then applied to a compound plate obtained by joining together

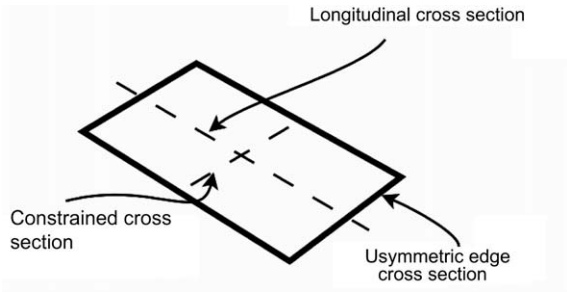

Fig. 12. Parametric study geometry and cross-sections.

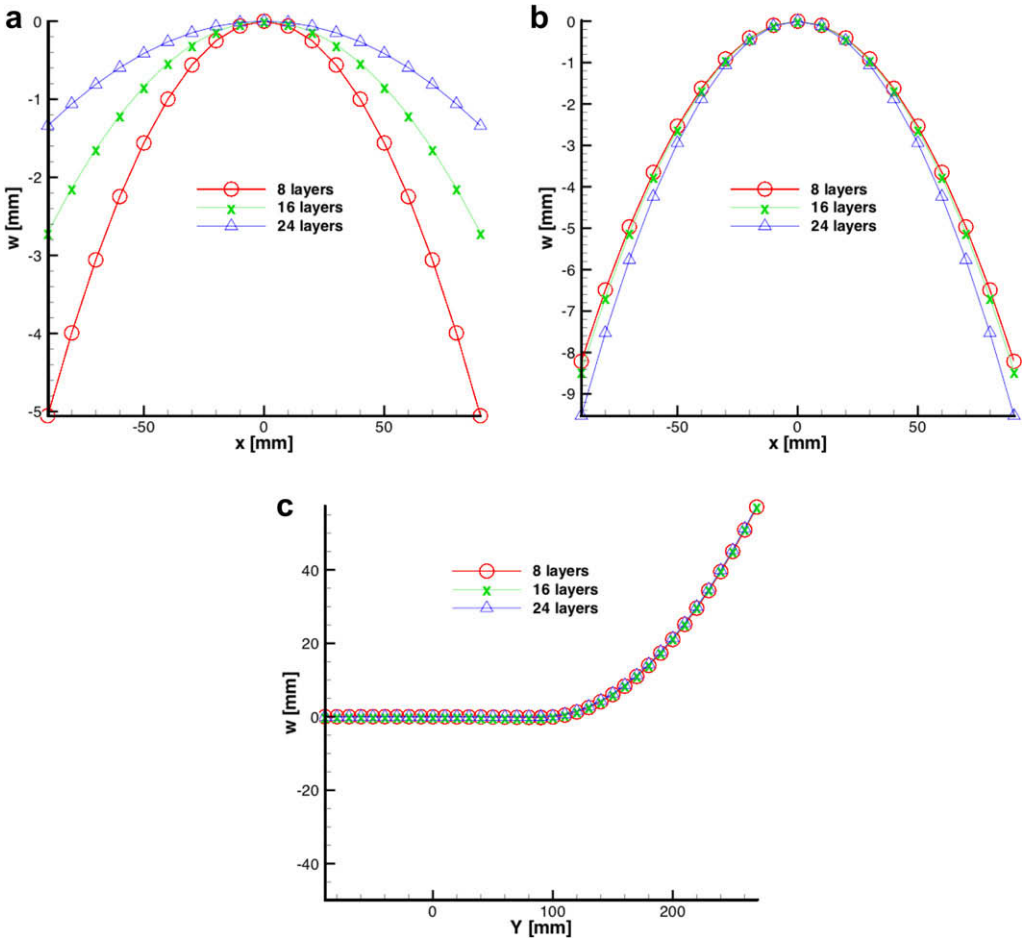

Fig. 13. Effects of the thickness of the symmetric part. (a) Constrained cross-section. (b) Unsymmetric edge cross-section. (c) Longitudinal cross-section for the curled configuration. (d) Effects of the stacking sequence of the symmetric part.

two square plates with symmetric and unsymmetric stacking sequences. The results obtained are compared with FEA and experimental tests achieving a satisfactory agreement. Finally, the technique is used to investigate the effects of the boundary conditions on the bi-stable behaviour of unsymmetric panels. It has been observed that if one edge is constrained, the curvature parallel to it is considerably reduced whereas the curvature perpendicular the edge remains almost unchanged. A parametric study performed by changing the thickness and the stacking sequence of the symmetric plate is used to confirm these results and to prove that the bi-stable behaviour of unsymmetric laminates is quite robust. This confirms that the integration of bi-stable patches within bigger structures could be a potential solution for the realisation of new structural systems where the requirement of flexibility and stiffness must be combined together.

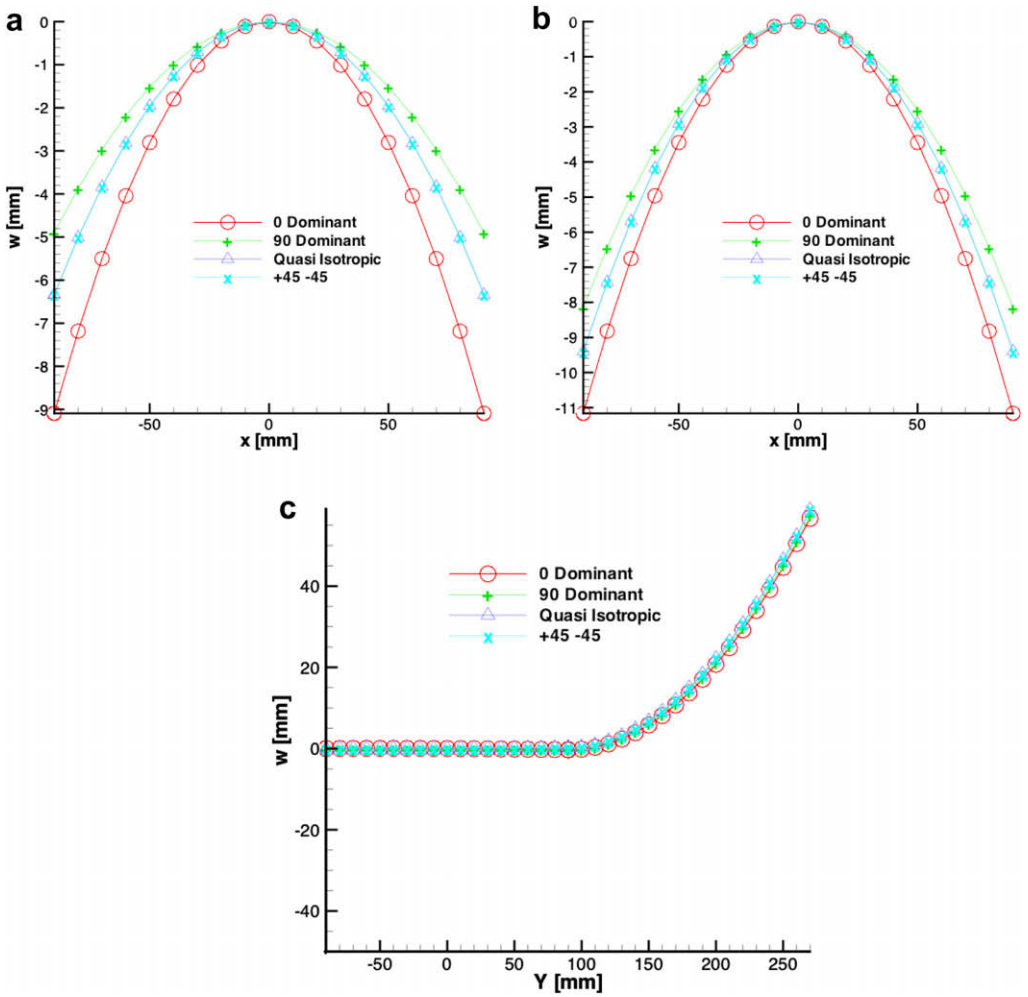

Fig. 14. (a) Constrained cross-section. (b) Unsymmetric edge cross-section. (c) Longitudinal cross-section for the curled configuration.

References

Diaconu, Cezar G., Weaver, Paul M., Mattioni, Filippo, 2008. Concepts for morphing airfoil sections using bi-stable laminated composite structures. Thin-Walled Structures 46 (6), 689–701.

Mattioni, F., Weaver, P., Friswell, M., Potter, K., 2007. Modeling and application of thermally induced multistable composites with piece-wise variation of lay-up in the planform. In: 15th AIAA/ASME/AHS Adaptive Structures Conference, April 23–26, Honolulu, Hawaii.

Mattioni, F., Weaver, P.M., Potter, K.D., Friswell, M.I., 2008. Analysis of thermally induced multistable composites. International Journal of Solids and Structures 45 (2), 657–675.

Hyer, M.W., 1982. The room-temperature shapes of four layer unsymmetric cross-ply laminates. Journal of Composite Materials 16, 318–340.

Hufenbach, W., Gude, M., 2002. Analysis and optimisation of multistable composites under residual stress. Composite structures 55, 319–327.

Iqbal, K., Pellegrino, S., 2000. Bi-stable composite shells. In: Proc. 41st AIAA/ASME/ASCE/AHS/ASC Structures, Structural Dynamics, and Materials Conference and Exhibit, 3–6 April 2000, Atlanta, GA, USA.

Jones, R.M., 1999. Mechanics of Composite Materials, second ed. Taylor & Francis, London.

Gigliotti, M., Wisnom, M.R., Potter, Kevin D., 2004. Loss of bifurcation and multiple shapes of thin [0/90] unsymmetric composite plates subject to thermal stress. Composites Science and Technology 64 (1), 109–128.

Dano, M.L., Hyer, M.W., 1998. Thermally-induced deformation behavior of unsymmetric laminates. International Journal of Solids and Structure 35 (17), 2101–2120.

Dano, M.L., Hyer, M.W., 2002. Snap-through of unsymmetric fiber-reinforced composite laminates. International Journal of Solids and Structures 39 (1), 175–198.

Dano, M.L., Hyer, M.W., 2003. SMA-induced snap-through of unsymmetric fiber-reinforced composite laminates. International Journal of Solids and Structures 40 (22), 5949–5972.

Hyer, M.W., Bhavani, P.C., 1984. Suppression of anticlastic curvature in isotropic and composite plate. International Journal of Solids and Structures 20 (6), 553–570.

Portela, P.M., Camanho, P.P., Weaver, P.M., Bond, I.P., 2008. Analysis of morphing, multistable structures actuated by piezoelectric patches. Computers and Structures 86, 347–356.

Potter, K.D., Weaver, P.M., 2004. A concept for the generation of out-of-plane distortion from tailored FRP laminates. Composites Part A: Applied Science and Manufacturing 35 (12), 1353–1361.

Schultz, M.R., 2008. A concept for airfoil-like active bistable twisting structures. Journal of Intelligent Material Systems and Structures 19 (2), 157–169. doi:10.1177/1045389X06073988.
Jun, W.J., Hong, C.S., 1990. Effect of residual shear strain on the cured shape of unsymmetric cross-ply thin laminates. Compos. Sci. Technol. 38, 55–67.